INORGANIC CHEMISTRY
FRONTIERS

RESEARCH ARTICLE

View Article Online
View Journal | View Issue

Check for updates

Cite this: *Inorg. Chem. Front.*, 2022, **9**, 4651

Cobalt sandwich-stabilized rhodium nanocatalysts for ammonia borane and tetrahydroxydiboron hydrolysis†

Qiuxia Zhao,[a,b] Bruno Espuche,[c,d] Naixin Kang,[a] Sergio Moya[c] and Didier Astruc*[a]

Received 20th June 2022,
Accepted 14th July 2022

DOI: 10.1039/d2qi01313d

rsc.li/frontiers-inorganic

Evolution of H_2 upon catalytic hydrolysis of inorganic hydrides is a key method for clean energy production. Here, a new organocobalt precursor is used to generate nanocatalysts that are efficient, stable and recyclable. The cobalt complexes [Co(η^5-C_5H_5)(η^4-C_5H_6)], **1**, and [Co(η^5-C_5Me_5)(η^4-C_5H_6)], **2**, are used to reduce late transition metal chlorides to a series of late transition metal nanoparticles, abbreviated TMNP and TMNP*, respectively, that catalyse hydrolysis of $B_2(OH)_4$ and ammonia borane (AB). Among the prepared TMNP and TMNP*, the latter are found to be the most efficient and recyclable catalysts, showing, with RhNP*, TOFs of 1364 mol_{H_2} mol_{cat}^{-1} min^{-1} in $B_2(OH)_4$ hydrolysis and 125 mol_{H_2} mol_{cat}^{-1} min^{-1} in AB hydrolysis at a low catalyst loading of 0.2 mol%. The kinetic study including kinetic isotope effect leads to a proposed mechanism of the RhNP*-catalysed AB hydrolysis involving water O–H bond oxidative addition on the catalyst surface as the rate-limiting step for H_2 generation.

1. Introduction

The conventional fossil fuels (coal, petroleum oil, and natural gas, *etc.*) produce dangerous greenhouse gas and considerable pollution, and therefore there is a huge demand for clean and sustainable energy sources.[1–5] Hydrogen gas (H_2) is regarded as the most attractive green energy source because of its high gravimetric energy density and lack of pollution due to its combustion product, water.[6–11] However, giving the dangers of explosion, large-scale application of H_2 involves transformation and storage issues. H_2 evolution from stable hydrogen storage materials appears as a valuable option. Boron chemistry contains hydrogen-rich compounds with hydridic hydrogen atoms,[12] and its role in energy-related processes has been very recently emphasized.[10] In particular, ammonia borane (AB) has attracted intensive attention owing to its high hydrogen content (19.6 wt%), high solubility and stability in aqueous solution.[13–32] Given the very low reaction rate of AB hydrolysis under ambient conditions, acceleration by catalysts is regarded as a promising way, and intensive efforts have been achieved to exploit efficient catalysts. It has been proposed that one of the hydrogen atoms of H_2 formed is provided by the borane group of AB, and the other one from water. Besides, the hydrolysis of tetrahydroxydiboron, $B_2(OH)_4$, is also promising for H_2 evolution as reported in the literature, but in this case it has been shown that both H atoms of H_2 are provided by water.[33–35] $B_2(OH)_4$ was first reported in 1955 by hydrolysis of B_2Cl_4 and $B_2(NMe_2)_4$.[36,37] Initially, the borylation of vinyl cyclopropane, vinyl aziridine, and allyl acetate substrates using $B_2(OH)_4$ was reported.[38] $B_2(OH)_4$ also serves as a reducing reagent, for example, for the reduction of pyridine-*N*-oxides[39] and nitro-aromatics.[40] Stokes and co-workers pioneered transfer hydrogenation of unsaturated hydrocarbons utilizing catalytic $B_2(OH)_4$ hydrolysis. Mechanistic studies revealed that $B_2(OH)_4$ facilitated the transfer of H atoms from water giving the intermediate Pd–H species, in which the unsaturated hydrocarbon inserted to complete its hydrogenation, and no H_2 gas was observed during the process.[41] Thus, $B_2(OH)_4$ plays the role of abstracting H atoms from water, rather than hydrogen storage material like AB.[34,42]

Transition-metal (TM) nanoparticles (NP) have multiple applications in optics, sensing and especially catalysis.[1,43–53] Active sites on their surface play a key role in binding substrate atoms due to their composition, size dispersity, morphology

[a]*ISM, UMR CNRS N° 5255, Univ. Bordeaux, 33405 Talence Cedex, France. E-mail: didier.astruc@u-bordeaux.fr*
[b]*LCC, CNRS & University of Toulouse III, 205 Route de Narbonne, 31077 Toulouse Cedex, France*
[c]*Soft Matter Nanotechnology Group, CIC biomaGUNE, Basque Research and Technology Alliance (BRTA), Paseo Miramón 182, 20014 San Sebastián, Guipúzcoa, Spain*
[d]*POLYMAT, Applied Chemistry Department, Faculty of Chemistry, University of the Basque Country, UPV/EHU, Paseo Manuel de Lardizabal 3, Donostia-San Sebastián, 20018, Spain*

†Electronic supplementary information (ESI) available. See DOI: https://doi.org/10.1039/d2qi01313d

and coordination by ligands.[54,55] The nanocatalysts are generally fabricated by reduction of TM salt precursors using a reducing agent such as $NaBH_4$, H_2, Mg, Li, Na naphthalene, *etc.*, in a presence of protecting ligand.[26,56–58] In this process, the oxidized form of the reductant is retained in an uncertain state, which is prone to disturb the coordination type between the nanocatalyst and ligands, consequently impacting the nanocatalyst activity and reliability.[59]

Hydride-rich organometallic complexes, obtained through reduction of 18-electron organometallic sandwich cations using sodium borohydride, have been studied as hydride-donating reagents for various chemical transformations.[60,61] For example, the hydride-rich complex [RhCp(η^4-C_5H_6)] was converted to rhodicenium cation in the presence of the hydride-accepting trityl (Ph_3C^+) cation *via* an initial electron-transfer step, followed by hydrogen-atom transfer, instead of a concerted hydride transfer.[60] Such a process is known in iron-sandwich chemistry.[62] The reverse has also long been known: reduction using $NaBH_4$ can proceed by electron transfer followed by H-atom transfer.[63] Barlow *et al.* reported two classes of organometallic hydride donors as *n*-dopants for organic semiconductors.[64] In cyclic voltammetry, organometallic hydrides undergo irreversible oxidation (**https://www-sciencedirect-com.inc.bib.cnrs.fr/topics/biochemistry-genetics-and-molecular-biology/alpha-oxidation**) that presumably involve single-electron oxidation followed by H atom transfer.[36,65]

Here, the hydride-rich neutral organometallics [Co(η^5-C_5H_5)(η^4-C_5H_6)], **1**, and [Co(η^5-C_5Me_5)(η^4-C_5H_6)], **2**, are used as reductants of transition metal chlorides, because upon reduction reactions these organocobalt complexes form cobalticenium chloride $\mathbf{1^+Cl^-}$, resp. pentamethylcobalticenium chloride $\mathbf{2^+Cl^-}$ that are well-characterized robust compounds. In the reduction process, they are expected to play both the role of reductants of M^{n+} to M^0 and that of NP stabilizer located around the NP periphery. NP stabilization is also insured by polyvinylpyrrolidone (PVP) 10 000. The resulting nanocatalysts are abbreviated TMNP (stabilized by **1**) and TMNP* (stabilized by **2**), respectively. A series of electron-reservoir and hydride-reservoir complexes [$CoCp_2$], [$FeCp_2$], [FeCp(η^5-C_6H_6)], [FeCp(η^5-C_6Me_6)], [CoCp(η^4-C_5H_6)], [FeCp(η^5-C_6H_7)], [FeCp(η^5-C_6Me_6H)], with Cp = η^5-C_5H_5, have already previously been used to stabilize AuNPs and PdNPs by their oxidized form.[66] It was concluded that [CoCp(η^4-C_5H_6)] gave better results than the above 19-electron electron-reservoir complexes and other 18-electron hydride-reservoir complexes in the catalysed reduction of 4-nitrophenol by AuNP and Suzuki–Miyaura coupling reaction catalysed by PdNP. We have retained the idea that hydride transfer appears superior to electron transfer for the catalytic efficacy of the generated NPs, and we are applying it for the first time to H_2 formation reactions. Another trend that we are investigating here is whether the use of the ligand η^5-C_5Me_5 (Cp*) in the Co complex instead of parent Cp is beneficial to catalysis. It is well known that permethylation of at least one Cp ligand stabilizes metallocenes and other organometallics because of the stereo-electronic influence of the five methyl substituents in Cp*. Indeed, Cp* is not only is much bulkier than the parent Cp, but also a much stronger electron-releasing ligand.[67] Here the synthesis of a series of nanomaterials TMNP* (TM = Rh, Pt, Pd, Au) using **2** as precursor for the reduction of TM chlorides is reported as well as their comparison with the related TMNP, prepared using **1**, in these two catalytic hydrogen evolution reactions.

2. Results and discussion

2.1. Preparation of TMNP and TMNP*

Metal precursors, for example, $RhCl_3$ (0.42 mg, 0.002 mmol), and PVP, 2 equiv., are dissolved in Milli-Q water (5 ml) under N_2 in a standard Schlenk flask and stirred for 30 min. Then, the freshly prepared complex [Co(η^5-C_5Me_5)(η^4-C_5H_6)] (**2**, 7.8 mg, 0.03 mmol, see ESI†) dissolved in THF is injected into the flask under N_2 atmosphere, and the colour of the solution changes immediately from colourless to dark brown, indicating the formation of RhNP* (eqn (1) and Fig. 1). After stirring for 30 min, the NPs are used in catalysis. The TMNP catalysts are prepared using the same method (see ESI†).

The reaction (eqn (1)) produces H_2, but both H atoms of H_2 in this case are provided by the hydridic atom of **2** (resp. **1**) previously added to $[CoCp^*Cp]^+$(resp. $[CoCp_2]^+$) upon reaction with $NaBH_4$.

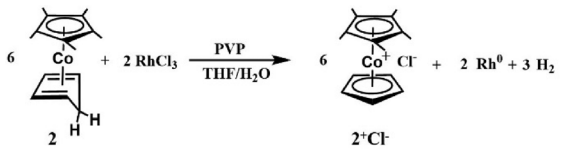

(1)

We suggest that **2** (resp. **1**) is oxidized by M^{n+} according to a single electron transfer yielding the isostructural, yet unstable, 17-electron complex $\mathbf{2^+}$ (resp. $\mathbf{1^+}$). There is then a considerable

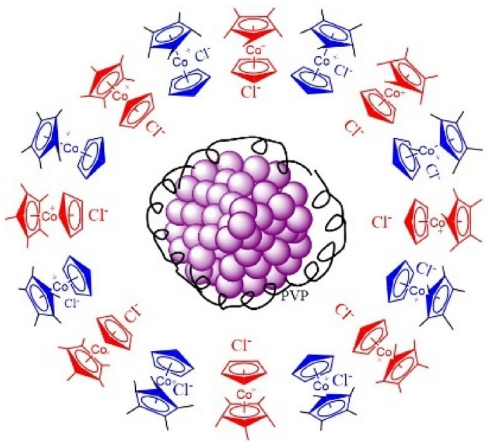

Fig. 1 Schematic illustration of the RhNP* catalyst synthesized upon reduction of $RhCl_3$ by [CoCp*(η^4-C_5H_6)]. The red colour shows coordination of Cl^- to the NP core, and the blue colour illustrates metallocenyl chloride without coordination, corresponding to Rh atoms in the core (that are thus not surface atoms).

driving force for transient $\mathbf{2}^+$ (resp. $\mathbf{1}^+$) to give the robust 18-electron cation $[CoCp^*Cp]^+$, (resp. $[CoCp_2]^+$), upon H-atom transfer probably to $M^{(n-1)+}$ in the course of its reduction process. The final H_2 formation might then result from reductive elimination from a $Rh(H)_2$ species formed by two successive H-atom transfers from two $\mathbf{2}^+$ (resp. $\mathbf{1}^+$) species. The alternative use of both electrons of the hydride to reduce M^{n+} while forming H^+ is energetically highly unlikely and finally experimentally discarded by the reaction stoichiometry, the evidence of H_2 formation, and the lack of acidity of the final aqueous medium.

These cobalt complexes and PVP function cooperatively to stabilize the NPs. Without PVP, the metal NPs immediately precipitate upon addition of the cobalt complex; thus, PVP serves as a NP steric stabilizer. The cationic cobalt complex serves as a NP electrostatic stabilizer (in conjunction with surface-coordinated Cl^-) and in the same time as a complementary remote steric protector of the NP surface. In a previous work, it was shown that, after the dialysis of the AuNP, the cobalt complex can be removed, because it is water soluble, and thus only PVP was left for the protection of Au nanoparticles. In that later case, however, AuNP that were only stabilized by PVP showed a sharply decreased catalytic activity (reaction rate declined from 22.7×10^{-3} s^{-1} to 3.1×10^{-3} s^{-1} in 4-nitrophenol reduction), because of the loss of this electrostatic protection by $[CoCp_2]^+$, Cl^-.[66]

2.2. Characterization of the nanoparticles

The microstructure and the size distribution of the TMNP* were investigated by transmission electron microscopy (TEM), and the typical catalysts RhNP* and AuNP* were examined. The characterization of this type of TMNP (including RhNP, but not RhNP*) is also accessible elsewhere.[66,68] As shown in Fig. 2A, the nanocatalyst RhNP* exhibits a diameter size of 2.5 ± 1.5 nm, while RhNP shows a larger diameter size of 3.0 ± 1.1 nm (Fig. S6†). As shown in Fig. 1, the small RhNP* are protected by ionic interactions between pentamethylcobalticenium chloride, $\mathbf{2}^+\mathbf{Cl}^-$, and the NPs surface. Faster reduction due to the better reducing agent with the strong donor Cp* compared to Cp is responsible for the formation of smaller RhNP* compared to RhNP.

The small AuNP* exhibit a diameter size distribution of 7.1 ± 3.5 nm (Fig. S7†). The CuNP* show a diameter of 10.1 ± 2.3 nm (Fig. S8†), which is the sign of the known weaker stability of the late first row TM NPs compared to the noble metal NP.

X-ray photoelectron spectroscopy (XPS) of RhNP* shows a bonding energy of 308.2 eV and 312.8 eV, which is assigned to Rh $3d_{5/2}$ and $3d_{3/2}$, respectively, indicating that Rh atoms at the surface of RhNP* are exclusively zero valent (Fig. 3). These Rh(0) values are close to those reported in the literature.[68,69] Very slightly higher values obtained here compared to the literature are attributable to the strong electrostatic effect provided by the ions of the organocobalt chloride complex surrounding the NP. In the UV-vis spectra of RhNP*, a band appears at 410 nm, corresponding to the pentamethylcobalticenium moiety, also indicating that organometallic reductants are oxidized by the Rh cations to form $\mathbf{2}^+\mathbf{Cl}^-$ and Rh(0) NPs (Fig. S9†).[66] As for AuNP*, besides the pentamethylcobalticenium peak at 410 nm, there is a broad absorbance at 520 nm corresponding to the surface plasmon band (SPB) of the AuNP*.

2.3. Catalytic performances of TMNP and TMNP* in the hydrolysis of $B_2(OH)_4$ and ammonia borane (AB)

2.3.1. Hydrolysis of $B_2(OH)_4$ catalysed by TMNP and TMNP*. Here, 0.2 mol% TMNP and TMNP* are used for $B_2(OH)_4$ hydrolysis. When 1 equiv. $B_2(OH)_4$ (90 mg) is consumed, 1 equiv. H_2 is produced, corresponding to 22.4 ml replacement of water in a typical water-filled gas burette at atmospheric pressure and room temperature (eqn (2)).[20]

$$B_2(OH)_4 + 2H - OH \rightarrow 2B(OH)_3 + H_2 \uparrow \quad (2)$$

The TMNP (TM = Rh, Pd, Pt) produced from **1**, termed RhNP, PdNP and PtNP, respectively (Fig. 4A), and the TMNP*, produced from **2** (Fig. 4C), are very active catalysts for $B_2(OH)_4$ hydrolysis. To compare the catalytic efficiency, the turnover frequency (TOF) is introduced here, defined as the number of moles of generated H_2 dividing by the total number of surface atoms over the time span of 10% substrate conversion. The calculated TOF values are 579 mol_{H_2} mol_{cat}^{-1} min^{-1} for RhNP, 138 mol_{H_2} mol_{cat}^{-1} min^{-1} for PdNP and 126 mol_{H_2} mol_{cat}^{-1}

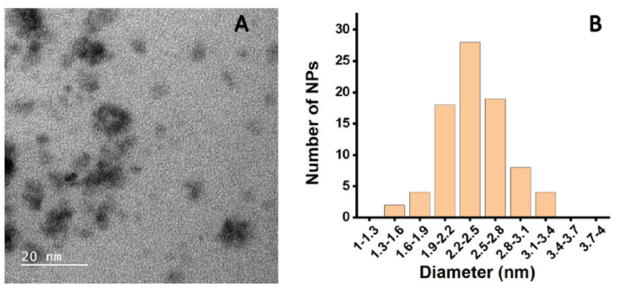

Fig. 2 TEM image (A) and size distribution (B) of the RhNPs*.

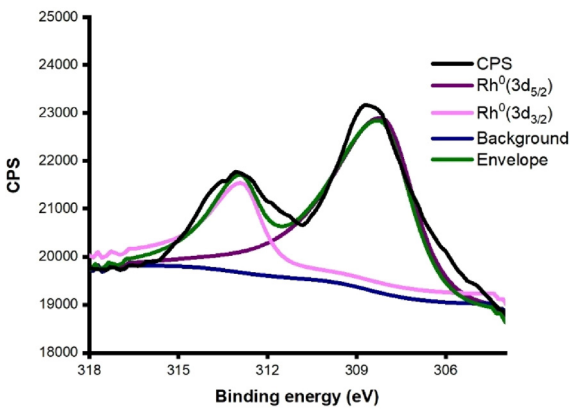

Fig. 3 XPS spectrum of the RhNP* (CPS: counts per second).

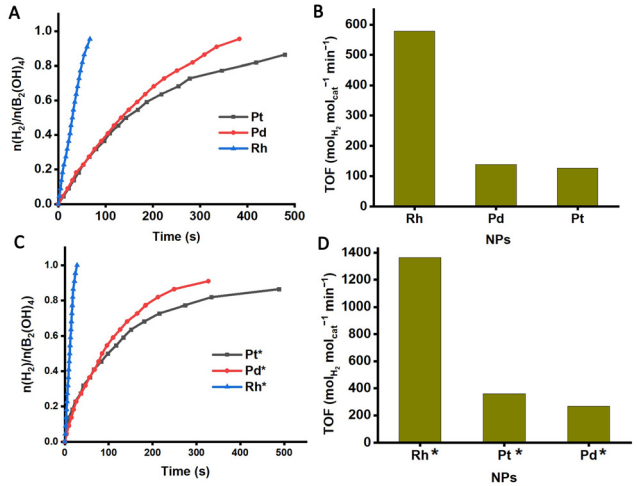

Fig. 4 Time plot of H_2 evolution from the hydrolysis of $B_2(OH)_4$ catalysed by TMNP (A) and TMNP* (C). TOF values of $B_2(OH)_4$ hydrolysis catalysed by TMNP (B) and TMNP* (D).

min^{-1} for PtNP, respectively (Fig. 4B), whereas the values are 1364 mol_{H_2} mol_{cat}^{-1} min^{-1} for RhNP*, 268 mol_{H_2} mol_{cat}^{-1} min^{-1} for PdNP* and 360 mol_{H_2} mol_{cat}^{-1} min^{-1} for PtNP*, respectively (Fig. 4D). The TOFs calculated by surface Rh atom (Table S1†) compare to those obtained with other stabilizers shown (Table S2†), revealing the very good activity of these RhNP*. Also, the results demonstrate that TMNP* exhibit a higher catalytic efficiency than their larger TMNP analogues. Besides, Rh is always the most active metal here among all the metals studied for catalytic $B_2(OH)_4$ hydrolysis with both organocobalt precursors.

The suggested mechanism in Scheme 1 follows the literature proposal involving oxidative addition of the B–B bond onto the NP surface followed by water coordination, β-H elimination and reductive elimination of the two hydride ligands to form H_2 in which both atoms come from water (Scheme 1).[34]

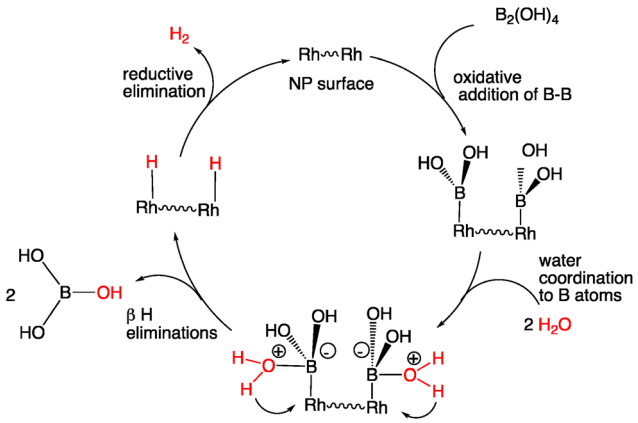

Scheme 1 Proposed mechanism for H_2 evolution upon RhNP*-catalyzed hydrolysis of $B_2(OH)_4$.

2.3.2. Ammonia borane hydrolysis catalysed by TMNP and TMNP*. To further compare the catalytic activities, the two groups of catalysts, TMNP and TMNP*, were then used for the hydrolysis of AB. AB is isoelectronic with gaseous ethane, but it shows different characteristics owing to the dipole moment between the N and B atoms. Its NH_3 and BH_3 fragments possess three protic $H^{\delta+}$ and three hydridic $H^{\delta-}$ hydrogens, respectively, which facilitates the intra-/inter-molecular $H^{\delta+}$–$H^{\delta-}$ interactions. Besides, AB is a solid under ambient conditions, which is attributed to the heteropolar dihydrogen bonding, making AB implementable as chemical hydrogen storage materials.[19] Typically, when 1 equiv. AB (31 mg) is hydrolysed with the assistance of 0.2 mol% catalyst loading in our case, 3 equiv. H_2 are produced (eqn (3)), resulting in 67 ml replacement of water in a water-filled gas burette at atmospheric pressure and room temperature.

$$NH_3BH_3 + 4H - OH \rightarrow NH_4{}^+B(OH)^-{}_4 + 3H_2 \uparrow \quad (3)$$

Time plots of H_2 evolution catalysed by TMNP are shown in Fig. 5A. Like for the catalytic $B_2(OH)_4$ hydrolysis, TMNP are also active for NH_3BH_3 hydrolysis, showing a TOF value of 165 mol_{H_2} mol_{cat}^{-1} min^{-1} for RhNP, 134 mol_{H_2} mol_{cat}^{-1} min^{-1} for PdNP and 141 mol_{H_2} mol_{cat}^{-1} min^{-1} for PtNP, respectively (Fig. 5B). For TMNP*, the TOF values are 125 mol_{H_2} mol_{cat}^{-1} min^{-1} for RhNP*, 21 mol_{H_2} mol_{cat}^{-1} min^{-1} for PdNP* and 67 mol_{H_2} mol_{cat}^{-1} min^{-1} PtNP*, respectively, *i.e.* somewhat lower for each metal compared with TMNP (Fig. 5C, D and Table 1), which is assigned to the protecting steric Cp* bulk decreasing the rate of substrate access to the NP surface. This order of catalytic activity at the beginning of the reactions, defined by the TOFs, between TMNP and TMNP* is opposite to that of the catalytic $B_2(OH)_4$ hydrolysis. On the other hand, when comparing the time plot of H_2 evolution in Fig. 5A and C, for example, RhNPs, the curve of RhNP bends with time going on, while the curve of RhNP* proceeds almost linearly during catalysis, indicating an efficiency decline of the catalyst

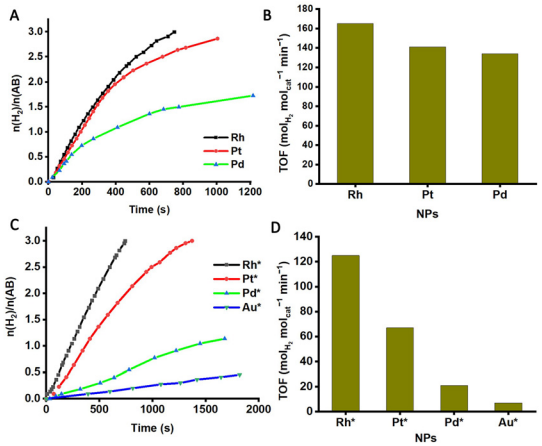

Fig. 5 Time plot of H_2 evolution from the hydrolysis of AB catalysed by TMNP (A) and TMNP* (C). TOF values of catalytic AB hydrolysis catalysed by TMNP (B) and TMNP* (D).

Table 1 Compared TOFs for $B_2(OH)_4$ and AB hydrolysis catalysed by nanoparticles supported by $\mathbf{1}^+$ and $\mathbf{2}^+$, respectively

	TOF $B_2(OH)_4$ hydrolysis		TOF AB hydrolysis	
	TMNP	TMNP*	TMNP	TMNP*
Rh	579	1364	165	125
Pd	138	268	134	21
Pt	126	360	141	67
Au	—	—	—	7

TOF: mol_{H_2} released at 10% H_2 yield/[total $mol_{catalyst}$ × reaction time (min)] for all atoms, the unit of TOF is $mol_{H_2}\ mol_{cat}^{-1}\ min^{-1}$.

in the former case, and a relatively stable state of RhNP* in the latter case of catalytic hydrolysis of AB. PtNP* and PdNP* also show almost linear time plots (Fig. 5C), whereas the time plot curves of PtNP and PdNP bend (Fig. 5A), indicating comparatively more stable PtNP* and PdNP* than PtNP and PdNP, respectively.

Besides, AuNP* exhibits catalytic activity in AB hydrolysis (Fig. 5C), whereas AuNP is inert at 0.2 mol% catalyst loading scale. In conclusion, although TMNP show a higher TOF value than TMNP* (except for Au), a better stability is obtained with TMNP*.

In sum, although the TMNP shows slightly higher TOF values than the TMNP* in AB hydrolysis (Tables 1 and S1†), **2** appears to be a preferred complex for the preparation of nanocatalysts, because it shows a fine balance between catalytic performance and stability. RhNP* favorably compares to the best state-of-the-art catalysts for AB hydrolysis in terms of TOF per surface atom, stability and recyclability (Table S3†).

These results also show that **2** is a better choice than **1** for the preparation of nanocatalysts. Subsequently, the reusability of the TMNP and TMNP* has been investigated. For the best RhNP in the parent TMNP family, the catalytic efficiency declined sharply in the second usage with only 1 mmol H_2 evolution in 1000 seconds along with precipitation of NPs in the hydrolysis of AB (Fig. 6A). On the other hand, RhNP* has been recycled 3 times with progressively increased reaction time and, importantly, no NP precipitation was observed after 3 cycles (Fig. 6B). These results confirm that the permethylated hydride reservoir complex **2** gives rise to a more satisfying catalyst than the analogue complex **1** concerning nanocatalyst stability and recyclability.

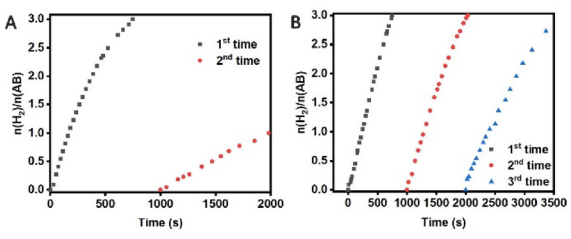

Fig. 6 Time plots of H_2 evolution from the hydrolysis of AB catalysed by RhNP (A) and RhNP*; (B) in the reuse test.

This difference of catalytic activity between TMNP and TMNP* can be ascribed to the methylation of the supporting ligands. In complex **2**, the Cp* ligand (Cp* = η^5-C_5Me_5) is as a stronger electron-donor than Cp (Cp = η^5-C_5H_5) owing to the existence of the 5 electron-releasing methyl groups in Cp*, which increases the electronic density of the central metal Co. Besides, the bulk of Cp* is considerably larger than that of Cp, offering a better steric protection than Cp for the NP stabilization. As a result, after the reduction of metal precursors, the NPs stabilized by $\mathbf{2}^+\mathbf{Cl}^-$ are more stable than those stabilized by $\mathbf{1}^+\mathbf{Cl}^-$.[67] The better stability of RhNP* compared to RhNP is an additional reason explaining the better catalytic results obtained with RhNP*, aggregation of NPs being better prevented with $\mathbf{2}^+\mathbf{Cl}^-$ than with $\mathbf{1}^+\mathbf{Cl}^-$. Better catalytic performance of TMNP* supported by $\mathbf{2}^+\mathbf{Cl}^-$ compared to TMNP supported by $\mathbf{1}^+\mathbf{Cl}^-$ in the catalytic hydrolysis of AB and $B_2(OH)_4$ result overall from both smaller NP size and better stability during the catalytic process.

2.4. Kinetic studies and mechanism

In order to investigate the mechanism of AB hydrolysis catalysed by TMNP*, the best catalyst RhNP* was used for kinetic studies. Fig. 7A shows the time plot of H_2 evolution in the presence of various concentrations of AB. The corresponding slop of logarithmic plot of H_2 evolution *vs.* AB concentration is 0.17 (Fig. 7B), indicating a zero-order kinetics in AB concentration. This also reveals that AB activation is barely involved in the rate-determining steps.[24]

The time plot of hydrogen evolution from AB hydrolysis catalysed by various amount of RhNP* is shown in Fig. 8A. Increasing the amount of catalyst is favourable for the acceleration of AB hydrolysis. The slop of logarithmic plot of H_2 generation *vs.* the amount of RhNP* is 0.97 (Fig. 8B), indicating that the reaction is first order in catalyst amount.

Fig. 9A depicts the temperature influence on AB hydrolysis catalysed by RhNP*; the H_2 evolution rate dramatically raises as the reaction temperature increases from 283K to 313K. From the Arrhenius plots in Fig. 9B, the activation energy (E_a) is calculated to be 26.1 kJ mol^{-1} according to the Arrhenius equation (eqn (S4)†).

When D_2O is used as solvent instead of H_2O for AB hydrolysis catalysed by 0.2% RhNP*, the result depicted in Fig. 10

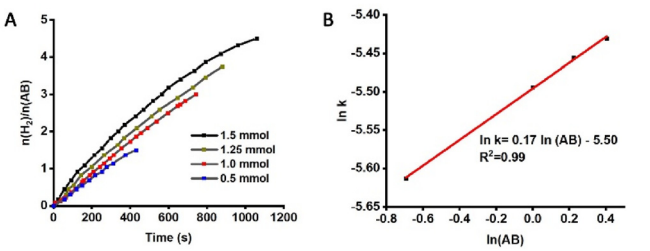

Fig. 7 (A) Time plots of H_2 evolution catalysed by 0.2 mol% RhNP* and (B) plots of the H_2 generation rate *vs.* AB concentration both on natural logarithmic scales.

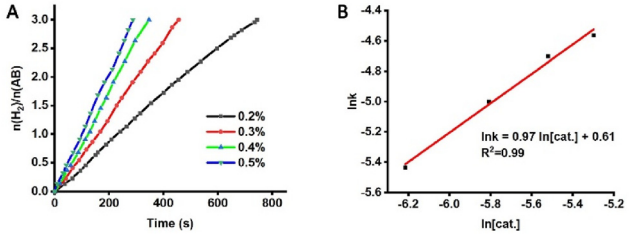

Fig. 8 (A) Plots of the times of the AB hydrolytic dehydrogenation catalysed by the RhNP* nanocatalyst with various catalyst amounts. (B) Plots of the rates of H_2 generation *vs.* concentration of the RhNP* nanocatalyst both on natural logarithmic scales.

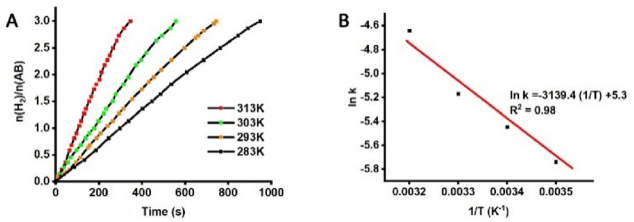

Fig. 9 (A) Plots of the hydrogen evolution *vs.* time for AB hydrolysis catalysed at various temperatures by 0.2 mol% RhNP* catalyst. (B) Kinetic data obtained from the Arrhenius plots.

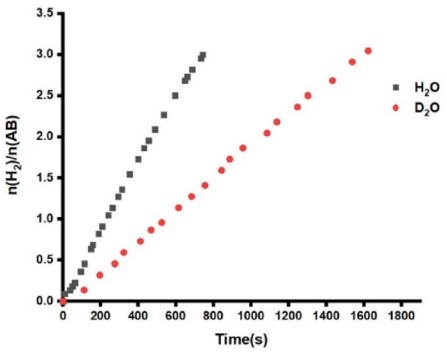

Fig. 10 Evolution of H_2 upon NH_3BH_3 hydrolysis with H_2O and D_2O catalysed by 0.2 mol% RhNP* (KIE = 2.3).

shows a decreased reaction rate in D_2O, indicating a kinetic isotope effect (KIE = k_D/k_H)[20,42] of 2.3, suggesting that the cleavage of the O–H bond in water is highly involved in the rate-determining step.

As the KIE experiment indicated that an O–H bond of water was cleaved in the rate-determining step, deuterated water was used in tandem reaction for further investigation of the atomic composition of the H_2 gas produced. In a tandem reaction, two chambers for different reactions were connected in a sealed system (Fig. 11). H_2 evolution occurred in the left chamber in the presence of AB (31 mg, 1 mmol), RhNP* (0.2% mmol) and D_2O (2 ml). Then, the produced H_2 gas transferred to the right chamber for the hydrogenation of styrene with the assistance of Pd/C and MeOD as solvent. After 24 h reaction at room temperature, the produced ethylbenzene was measured

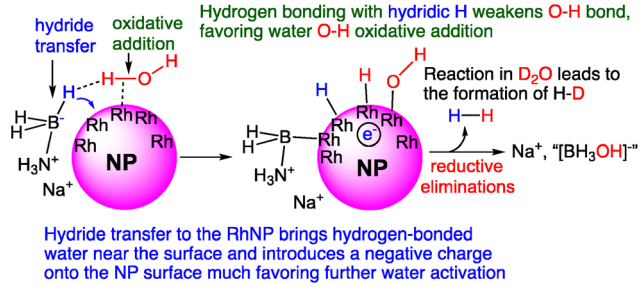

Fig. 11 Schematized mechanism for the formation of the first H_2 molecule upon RhNP-catalyzed AB hydrolysis. Formation of the 3 H2 molecules is summarized in Fig. 12.

by ^{1}H NMR for confirmation. As shown in Fig. S10,† the integration of the ^{1}H NMR peaks at 7.12–7.28 ppm and 1.21–1.25 ppm is 5.00 and 3.03, respectively, corresponding to the phenyl and methyl groups. The peaks at 2.67–2.58 ppm, that are assigned to methylene group, show an integration of 0.84, less than the expected 2.00, indicating one D substitution in ethylbenzene. From the ^{1}H NMR of isotopic ethylbenzene, it is suggested that one H atom of the produced H_2 comes from water, and another H atom comes from AB in the hydrolysis of AB catalysed by RhNP*, confirming previous publications.

Based on the experimental result above, the mechanism confirms trends that were previously suggested. Owing to the hydridic property of B–H bond, water is prone to form $[NH_3BH_2H]\cdots$H–OH complex with NH_3BH_3 *via* H bonding, which weakens the AB hydridic B–H bond and water O–H bond. Hydride transfer from AB to the nanocatalyst surface leads to B–H bond cleavage and formation of a negatively charged surface M–H species. The above H bonding with water bring water nearby the nanocatalyst surface, which very much facilitates water O–H cleavage (rate-determining step), and all the more so that electron density in this bond is weakened by this H bonding and the NP is more active in oxidative addition due to higher electron density brought by the negative charge. As a result, the first H_2 molecule is produced by reductive elimination of two surface hydrides, leaving on the NP surface two fragments, $NH_3BH_2^-$ and OH^- that also reductively eliminate, which provides the reaction intermediate NH_3BH_2OH (Fig. 11). Repetition of this process schematized in Fig. 11, finally gives evolution of 3 equiv. H_2 (Fig. 12).

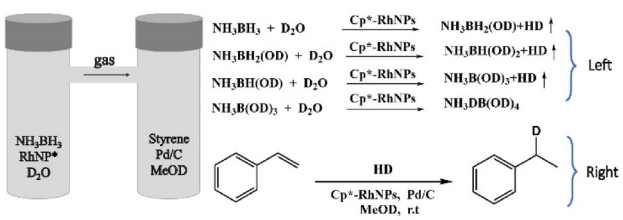

Fig. 12 Tandem reaction of AB dehydrogenation in D_2O and hydrogenation of styrene in MeOD.

3. Conclusions

The TMNP and TMNP*, prepared from the reduction of late TM chloride salts by hydride-rich cobaltocene derivatives $[Co(\eta^5\text{-}C_5H_5)(\eta^4\text{-}C_5H_6)]$, **1**, resp. $[Co(\eta^5\text{-}C_5Me_5)(\eta^4\text{-}C_5H_6)]$, **2**, have been characterized. They are used for the first time to carry out two catalytic H_2 evolution reactions using hydrolysis of both ammonia borane and $B_2(OH)_4$. The results reveal that the Rh nanocatalysts prepared in this way are among the best nanocatalysts for these reactions. For instance, they compare advantageously with previous nanocatalysts prepared using dendrimers[70,71] or metal organic frameworks.[53,72] RhNP* show a catalytic activity (TOF) superior to that of RhNP for $B_2(OH)_4$ hydrolysis, and this trend is opposite for AB hydrolysis whose reaction mechanism is very different (in AB hydrolysis, one H atom of H_2 comes from AB and the other ones from water, whereas in $B_2(OH)_4$ hydrolysis both H atoms of H_2 are provided by water). However, the activity of RhNP decreases in the course of the reactions due to lack of sufficient stability, and this RhNP is not recyclable due to aggregation. On the other hand, the TMNP* are stable nanocatalysts in the course of reactions, which is assigned to the steric bulk of the Cp* ligand of the organocobalt cation protecting the nanocatalyst surface. The RhNP* appear stable and recyclable at least three times without agglomeration; they are the best choice for the hydrolysis of both AB and $B_2(OH)_4$, and the catalytic results are good compared to the literature. Kinetic studies of AB dehydrogenation catalysed by RhNP* revealed that the reaction is zero order in AB concentration and first order in NP amount with a low activation energy E_a of 26.1 kJ mol^{-1}. The KIE value of 2.3 indicates that the O–H cleavage of water is highly involved in the rate-determining step, proposed to be much facilitated by H bonding between AB and water. This first and successful use of the new complex **2** to produce efficient nanocatalysts upon reduction of TM salts could in the future be extended to other catalytic systems. Great advantages of the use of these neutral hydridic cobalt complexes are their strong reducing power as hydride donors (still increased with the better electron donor ligand Cp*), their use as both reductant and NP stabilizer with steric protection (still increased with the large Cp*), and the fact that their oxidized forms are fully stable and easily recovered as water soluble chloride salts. The catalytic performances are among the best ones compared to previous results, and this strategy should also allow further stabilization and catalytic use of the NPs on various other supports.

Author contributions

Q. Z.: Data curation, formal analysis, investigation, software, visualization, validation, writing – original draft; B. E.: Investigation, software and formal analysis of TEM and PES; N. K.: Part of investigation; S. M.: Funding acquisition and formal analysis of TEM and PES; D. A.: Conceptualization, funding acquisition, supervision, writing – review and editing.

Conflicts of interest

The authors declare no conflict of interest.

Acknowledgements

Financially support from the China Scholarship Council (CSC, PhD grants to Q. Z. and N. K.), the PID2020-114356RB-I00 Retos Project from the Ministerio de Economía, Industria y Competitividad, gobierno de España (S. M.), the Centre National de la Recherche Scientifique (CNRS) and the University of Bordeaux is gratefully acknowledged.

Notes and references

1 REN21, Renewables 2018 Global Status Report, 2018, https://www.ren21.net/about-ren21/about-us/.
2 S. Chu and A. Majumdar, Opportunities and challenges for a sustainable energy future, *Nature*, 2012, **488**, 294–303.
3 J. Zhu, L. Hu, P. Zhao, L. Y. S. Lee and K. Y. Wong, Recent Advances in Electrocatalytic Hydrogen Evolution Using Nanoparticles, *Chem. Rev.*, 2020, **120**, 851–918.
4 N. S. Lewis and D. G. Nocera, Powering the planet: Chemical challenges in solar energy utilization, *Proc. Natl. Acad. Sci. U. S. A.*, 2006, **103**, 15729–15735.
5 B. Ates, S. Koytepe, A. Ulu, C. Gurses and V. K. Thakur, Chemistry, Structures, and Advanced Applications of Nanocomposites from Biorenewable Resources, *Chem. Rev.*, 2020, **120**, 9304–9362.
6 T. He, P. Pachfule, H. Wu, Q. Xu and P. Chen, Hydrogen Carriers, *Nat. Rev. Mater.*, 2016, **1**, 16059.
7 Y. Tachibana, L. Vayssieres and J. R. Durrant, Artificial photosynthesis for solar water-splitting, *Nat. Photonics*, 2012, **6**, 511–518.
8 S. E. Hosseini and M. A. Wahid, Hydrogen production from renewable and sustainable energy resources: Promising green energy carrier for clean development, *Renewable Sustainable Energy Rev.*, 2016, **57**, 850–866.
9 P. Nikolaidis and A. Poullikkas, A comparative overview of hydrogen production processes, *Renewable Sustainable Energy Rev.*, 2017, **67**, 597–611.
10 Z. Huang, S. Wang, R. D. Dewhurst, N. V. Ignat'ev, M. Finze and H. Braunschweig, Boron: Its Role in Energy-Related Processes and Applications, *Angew. Chem., Int. Ed.*, 2020, **59**, 8800–8816.
11 J. Shen, W. Chen, G. Lv, Z. Yang, J. Yan, X. Liu and Z. Dai, Hydrolysis of NH_3BH_3 and $NaBH_4$ by graphene quantum dots-transition metal nanoparticles for highly effective hydrogen evolution, *Int. J. Hydrogen Energy*, 2021, **46**, 796–805.
12 Q. Zhao, R. D. Dewhurst, H. Braunschweig and X. Chen, A New Perspective on Borane Chemistry: The Nucleophilicity of the B–H Bonding Pair Electrons, *Angew. Chem., Int. Ed.*, 2019, **58**, 3268–3278.

13 A. Staubitz, A. P. M. Robertson and I. Manners, *Chem. Rev.*, 2010, **110**, 4079–4124.
14 Z. Li, T. He, D. Matsumura, S. Miao, A. Wu, L. Liu, G. Wu and P. Chen, Atomically Dispersed Pt on the Surface of Ni Particles: Synthesis and Catalytic Function in Hydrogen Generation from Aqueous Ammonia–Borane, *ACS Catal.*, 2017, **7**, 6762–6769.
15 D. W. Himmelberger, C. W. Yoon, M. E. Bluhm, P. J. Carroll and L. G. Sneddon, Base-Promoted Ammonia Borane Hydrogen-Release, *J. Am. Chem. Soc.*, 2009, **131**, 14101–14110.
16 H. Wu, Y. Cheng, B. Wang, Y. Wang, M. Wu, W. Li, B. Liu and S. Lu, Carbon dots-confined CoP-CoO nanoheterostructure with strong interfacial synergy triggered the robust hydrogen evolution from ammonia borane, *J. Energy Chem.*, 2021, **57**, 198–205.
17 W. Chen, X. Duan, G. Qian, D. Chen and X. Zhou, Carbon Nanotubes as Support in the Platinum-Catalyzed Hydrolytic Dehydrogenation of Ammonia Borane, *ChemSusChem*, 2015, **8**, 2927–2931.
18 S. Akbayrak, Y. Tonbul and S. Özkar, Ceria supported rhodium nanoparticles: Superb catalytic activity in hydrogen generation from the hydrolysis of ammonia borane, *Appl. Catal., B*, 2016, **198**, 162–170.
19 W. W. Zhan, Q. L. Zhu and Q. Xu, Dehydrogenation of Ammonia Borane by Metal Nanoparticle Catalysts, *ACS Catal.*, 2016, **6**, 6892–6905.
20 Q. Wang, F. Fu, S. Yang, M. M Moro, M. d. l. A. Ramirez, S. Moya, L. Salmon, J. Ruiz and D. Astruc, Dramatic Synergy in CoPt Nanocatalysts Stabilized by "Click" Dendrimers for Evolution of Hydrogen from Hydrolysis of Ammonia Borane, *ACS Catal.*, 2018, **9**, 1110–1119.
21 P. Xu, W. Lu, J. Zhang and L. Zhang, Efficient Hydrolysis of Ammonia Borane for Hydrogen Evolution Catalyzed by Plasmonic Ag@Pd Core–Shell Nanocubes, *ACS Sustainable Chem. Eng.*, 2020, **8**, 12366–12377.
22 S. Rej, C. F. Hsia, T. Y. Chen, F. C. Lin, J. S. Huang and M. H. Huang, Facet-Dependent and Light-Assisted Efficient Hydrogen Evolution from Ammonia Borane Using Gold–Palladium Core–Shell Nanocatalysts, *Angew. Chem., Int. Ed.*, 2016, **55**, 7222–7226.
23 Y. Wu, Y. Sun, W. Fu, X. Meng, M. Zhu, S. Ramakrishna and Y. Dai, Graphene-Based Modulation on the Growth of Urchin-like $Na_2Ti_3O_7$ Microspheres for Photothermally Enhanced H_2 Generation from Ammonia Borane, *ACS Appl. Nano Mater.*, 2020, **3**, 2713–2722.
24 F. Fu, C. Wang, Q. Wang, A. M. Martinez-Villacorta, A. Escobar, H. Chong, X. Wang, S. Moya, L. Salmon, E. Fouquet, J. Ruiz and D. Astruc, Highly Selective and Sharp Volcano-type Synergistic Ni_2Pt@ZIF-8-Catalyzed Hydrogen Evolution from Ammonia Borane Hydrolysis, *J. Am. Chem. Soc.*, 2018, **140**, 10034–10042.
25 C. Wang, J. Tuninetti, Z. Wang, C. Zhang, R. Ciganda, L. Salmon, S. Moya, J. Ruiz and D. Astruc, Hydrolysis of Ammonia-Borane over Ni/ZIF-8 Nanocatalyst: High Efficiency, Mechanism, and Controlled Hydrogen Release, *J. Am. Chem. Soc.*, 2017, **139**, 11610–11615.
26 J. M. Yan, X. B. Zhang, S. Han, H. Shioyama and Q. Xu, Iron-nanoparticle-catalyzed hydrolytic dehydrogenation of ammonia borane for chemical hydrogen storage, *Angew. Chem., Int. Ed.*, 2008, **47**, 2287–2289.
27 W. Chen, D. Li, C. Peng, G. Qian, X. Duan, D. Chen and X. Zhou, Mechanistic and Kinetic Insights into the Pt-Ru Synergy during Hydrogen Generation from Ammonia Borane over PtRu/CNT Nanocatalysts, *J. Catal.*, 2017, **356**, 186–196.
28 K. Mori, K. Miyawaki and H. Yamashita, Ru and Ru-Ni Nanoparticles on TiO_2 Support as Extremely Active Catalysts for Hydrogen Production from Ammonia-Borane, *ACS Catal.*, 2016, **6**, 3128–3135.
29 L. Wang, H. Li, W. Zhang, X. Zhao, J. Qiu, A. Li, X. Zheng, Z. Hu, R. Si and J. Zeng, Supported Rhodium Catalysts for Ammonia–Borane Hydrolysis: Dependence of the Catalytic Activity on the Highest Occupied State of the Single Rhodium Atoms, *Angew. Chem., Int. Ed.*, 2017, **56**, 4712–4718.
30 H. Cheng, T. Kamegawa, K. Mori and H. Yamashita, Surfactant-free nonaqueous synthesis of plasmonic molybdenum oxide nanosheets with enhanced catalytic activity for hydrogen generation from ammonia borane under visible light, *Angew. Chem., Int. Ed.*, 2014, **53**, 2910–2914.
31 J. Zhang, W. Chen, H. Ge, C. Chen, W. Yan, Z. Gao, J. Gan, B. Zhang, X. Duan and Y. Qin, Synergistic Effects in Atomic-layer-deposited PtCox/CNTs Catalysts Enhancing Hydrolytic Dehydrogenation of ammonia Borane, *Appl. Catal., B*, 2018, **235**, 256–263.
32 L. Yin, T. Zhang, K. Dai, B. Zhang, X. Xiang and H. Shang, Ultrafine PtCo Alloy Nanoclusters Confined in N-Doped Mesoporous Carbon Spheres for Efficient Ammonia Borane Hydrolysis, *ACS Sustainable Chem. Eng.*, 2021, **9**, 822–832.
33 Q. Zhao, N. Kang, M. M. Moro, E. Guisasola, S. Moya, E. Coy, L. Salmon, X. Liu and D. Astruc, Sharp Volcano-Type Synergy and Visible Light Acceleration in H_2 Release upon $B_2(OH)_4$ Hydrolysis Catalyzed by Au-Rh@Click-Dendrimer Nanozymes, *ACS Appl. Energy Mater.*, 2022, **5**, 3834–3844.
34 W. Chen, J. Shen, Y. Huang, X. Liu and D. Astruc, Catalyzed Hydrolysis of Tetrahydroxydiboron by Graphene Quantum Dot-Stabilized Transition-Metal Nanoparticles for Hydrogen Evolution, *ACS Sustainable Chem. Eng.*, 2020, **8**, 7513–7522.
35 J. Zhou, Y. Huang, J. Shen and X. Liu, Pd/C-Catalyzed H2 Evolution from Tetrahydroxydiboron Hydrolysis, *Catal. Lett.*, 2021, **151**, 3004–3010.
36 T. Wartik and E. F. Apple, A New Modification of Boron Monoxide, *J. Am. Chem. Soc.*, 1955, **77**, 6400–6401.
37 Z.-Y. Sun, S. Zhou, K. Yang, M. Guo, W. Zhao, X. Tang and G. Wang, Tetrahydroxydiboron-Promoted Radical Addition of Alkynols, *Org. Lett.*, 2020, **22**, 6214–6219.
38 S. Sebelius, V. J. Olsson and K. J. Szabó, Palladium Pincer Complex Catalyzed Substitution of Vinyl Cyclopropanes, Vinyl Aziridines, and Allyl Acetates with Tetrahydroxydiboron. An Efficient Route to Functionalized

Allylboronic Acids and Potassium Trifluoro(allyl)borates, *J. Am. Chem. Soc.*, 2005, **127**, 10478–10479.

39 A. T. Londregan, D. W. Piotrowski and J. Xiao, Rapid and Selective in situ Reduction of Pyridine-N-oxides with Tetrahydroxydiboron, *Synlett*, 2013, **24**, 2695–2700.

40 D. Y. Chen, Y. M. Zhou, H. F. Zhou, S. S. Liu, Q. X. Liu, K. L. Zhang and Y. Uozumi, Metal-free Reduction of Nitro Aromatics to Amines with $B_2(OH)_4/H_2O$, *Synlett*, 2018, **29**, 1765–1768.

41 S. P. Cummings, T. N. Le, G. E. Fernandez, L. G. Quiambao and B. J. Stokes, Tetrahydroxydiboron-Mediated Palladium-Catalyzed Transfer Hydrogenation and Deuteriation of Alkenes and Alkynes Using Water as the Stoichiometric H or D Atom Donor, *J. Am. Chem. Soc.*, 2016, **138**, 6107–6110.

42 M. Gomez-Gallego and M. A. Sierra, Kinetic isotope effects in the study of organometallic reaction mechanisms, *Chem. Rev.*, 2011, **111**, 4857–4963.

43 C. B. Murray, C. R. Kagan and M. G. Bawendi, Synthesis and Characterization of Monodisperse Nanocrystals and Close-Packed Nanocrystal Assemblies, *Annu. Rev. Mater. Sci.*, 2000, **30**, 545–610.

44 M.-C. Daniel and D. Astruc, Gold Nanoparticles: Assembly, Supramolecular Chemistry, Quantum-Size-Related Properties, and Applications toward Biology, Catalysis, and Nanotechnology, *Chem. Rev.*, 2004, **104**, 293–346.

45 P. Hervés, M. Pérez-Lorenzo, L. M. Liz-Marzán, J. Dzubiella, Y. Lu and M. Ballauff, Catalysis by metallic nanoparticles in aqueous solution: model reactions, *Chem. Soc. Rev.*, 2012, **41**, 5577–5587.

46 X.-F. Yang, A. Wang, B. Qiao, J. Li, J. Liu and T. Zhang, Single-Atom Catalysts: A New Frontier in Heterogeneous Catalysis, *Acc. Chem. Res.*, 2013, **46**, 1740–1748.

47 D. Wang and D. Astruc, Fast-Growing Field of Magnetically Recyclable Nanocatalysts, *Chem. Rev.*, 2014, **114**, 6949–6985.

48 M. L. Brongersma, N. J. Halas and P. Nordlander, Plasmon-induced hot carrier science and technology, *Nat. Nanotechnol.*, 2015, **10**, 25–34.

49 D. Wang and D. Astruc, The recent development of efficient Earth-abundant transition-metal nanocatalysts, *Chem. Soc. Rev.*, 2017, **46**, 816–854.

50 L. Liu and A. Corma, Metal Catalysts for Heterogeneous Catalysis: From Single Atoms to Nanoclusters and Nanoparticles, *Chem. Rev.*, 2018, **118**, 4981–5079.

51 D. Astruc, Introduction: Nanoparticles in Catalysis, *Chem. Rev.*, 2020, **120**, 461–463.

52 S. Ji, Y. Chen, X. Wang, Z. Zhang, D. Wang and Y. Li, Chemical Synthesis of Single Atomic Site Catalysts, *Chem. Rev.*, 2020, **120**, 11900–11955.

53 Q. Wang and D. Astruc, State of the Art and Prospects in Metal-Organic Framework (MOF)-Based and MOF-Derived Nanocatalysis, *Chem. Rev.*, 2020, **120**, 1438–1511.

54 L. Nguyen, F. F. Tao, Y. Tang, J. Dou and X.-J. Bao, Understanding Catalyst Surfaces during Catalysis through Near Ambient Pressure X-ray Photoelectron Spectroscopy, *Chem. Rev.*, 2019, **119**, 6822–6905.

55 Z. Zheng, H. Li, T. Liu and R. Cao, Monodisperse noble metal nanoparticles stabilized in SBA-15: Synthesis, characterization and application in microwave-assisted Suzuki–Miyaura coupling reaction, *J. Catal.*, 2010, **270**, 268–274.

56 D. Astruc, F. Lu and J. R. Aranzaes, Nanoparticles as Recyclable Catalysts: The Frontier between Homogeneous and Heterogeneous Catalysis, *Angew. Chem., Int. Ed.*, 2005, **44**, 7852–7872.

57 C. Schöttle, P. Bockstaller, R. Popescu, D. Gerthsen and C. Feldmann, Sodium-Naphthalenide-Driven Synthesis of Base-Metal Nanoparticles and Follow-up Reactions, *Angew. Chem., Int. Ed.*, 2015, **54**, 9866–9870.

58 C. Schöttle, D. E. Doronkin, R. Popescu, D. Gerthsen, J.-D. Grunwaldt and C. Feldmann, Ti0 nanoparticles via lithium-naphthalenide-driven reduction, *Chem. Commun.*, 2016, **52**, 6316–6319.

59 F. Fu, R. Ciganda, Q. Wang, A. Tabey, C. Wang, A. Escobar, A. M. Martinez-Villacorta, R. Hernández, S. Moya, E. Fouquet, J. Ruiz and D. Astruc, Cobaltocene Reduction of Cu and Ag Salts and Catalytic Behavior of the Nanoparticles Formed, *ACS Catal.*, 2018, **8**, 8100–8106.

60 S. Zhang, K. Moudgil, E. Jucov, C. Risko, T. V. Timofeeva, S. R. Marder and S. Barlow, Organometallic hydride-transfer agents as reductants for organic semiconductor molecules, *Inorg. Chim. Acta*, 2019, **489**, 67–77.

61 N. G. Connelly and W. E. Geiger, Chemical Redox Agents for Organometallic Chemistry, *Chem. Rev.*, 1996, **96**, 877–910.

62 D. Mandon, L. Toupet and D. Astruc, Electron-Transfer Pathways in the Hydride Abstraction by Ph_3C^+ from Exo-Substituted Cyclohexadiene Fe(0) Complexes : A Key in the Synthesis of Heterobifunctional Cyclohexadienes from Benzene, *J. Am. Chem. Soc.*, 1986, **108**, 1320–1321.

63 P. Michaud, D. Astruc and J. H. Ammeter, Electon-Transfer Pathways in the Reduction of d^6 and d^7 Organo-Iron Cations by $LiAlH_4$ and $NaBH_4$, *J. Am. Chem. Soc.*, 1982, **104**, 3755–3757.

64 B. D. Naab, S. Guo, S. Olthof, E. G. B. Evans, P. Wei, G. L. Millhauser, A. Kahn, S. Barlow, S. R. Marder and Z. Bao, Mechanistic Study on the Solution-Phase *n*-Doping of 1,3-Dimethyl-2-aryl-2,3-dihydro-1H-benzoimidazole Derivatives, *J. Am. Chem. Soc.*, 2013, **135**, 15018–15025.

65 X. Han, W. Hao, X.-Q. Zhu and V. D. Parker, A Thermodynamic and Kinetic Study of Hydride Transfer of a Caffeine Derivative, *J. Org. Chem.*, 2012, **77**, 6520–6529.

66 F. Fu, Q. Wang, R. Ciganda, A. M. Martinez-Villacorta, A. Escobar, S. Moya, E. Fouquet, J. Ruiz and D. Astruc, Electron- and Hydride-Reservoir Organometallics as Precursors of Catalytically Efficient Transition Metal Nanoparticles in Water, *Chem. – Eur. J.*, 2018, **24**, 6645–6653.

67 X. Meng, C. Ma, L. Jiang, R. Si, X. Meng, Y. Tu, L. Yu, X. Bao and D. Deng, Distance Synergy of MoS_2-Confined Rhodium Atoms for Highly Efficient Hydrogen Evolution, *Angew. Chem.*, 2020, **132**, 10588–10593.

68 W. Wang, R. Ciganda, C. Wang, A. Escobar, A. M. Martinez-Villacorta and M. de los Angeles Ramirez, Ricardo Hernandez, S. E. Moya, J. Ruiz, J.-R. Hamon and D. Astruc, High catalytic activity of Rh nanoparticles generated from cobaltocene and $RhCl_3$ in aqueous solution, *Inorg. Chem. Front.*, 2019, **6**, 2704–2708.

69 D. Astruc, *Organometallic Chemistry and Catalysis*, Springer, Berlin, 2007.

70 M. C. Daniel, J. Ruiz, N. Dro and D. Astruc, Synthesis of five generations of redox-stable pentamethyl-amidoferrocenyl dendrimers, *Chem. – Eur. J.*, 2003, **9**, 4371–4379.

71 D. Astruc, Electron-transfer processes in dendrimers and their implication in biology, catalysis, sensing and nanotechnology, *Nat. Chem.*, 2012, **4**, 255–267.

72 C. L. Wang, Q. Wang, F. Fu and D. Astruc, Hydrogen Generation upon Nanocatalyzed Hydrolysis of Hydrogen-Rich Boron Derivatives: Recent Developments, *Acc. Chem. Res.*, 2020, **53**, 2483–2493.